Available online at www.sciencedirect.com
SCIENCE DIRECT®

Polymer 44 (2003) 3299–3307

polymer
www.elsevier.com/locate/polymer

Molecular dynamics of chiral semi-crystalline poly(*R*)-(3-hydroxyalkanoates)

Man Ken Cheung[a,*], P. Gao[b], Si Wan Li[b]

[a]*Open Laboratory of Chirotechnology of the Institute of Molecular Technology for Drug Discovery and Synthesis, Department of Applied Biology and Chemical Technology, Hong Kong Polytechnic University, Hung Hom, Kowloon, Hong Kong, People's Republic of China*
[b]*Department of Chemical Engineering, Hong Kong University of Science and Technology, Clear Water Bay, Kowloon, Hong Kong, People's Republic of China*

Received 9 December 2002; received in revised form 24 February 2003; accepted 26 February 2003

Abstract

The inversion-recovery cross-polarization (IRCP) sequence used for measuring cross-relaxation time (T_{CH}) is modified to obtain signals that show exponential or spin-lock (SL) decay to zero. The new sequence may, therefore, be analogously abbreviated as SLCP. Poly(*R*)-(3-hydroxybutyrate-*co*-3-hydroxyhexanoate) {P(HB-HHx) (85:15)} is found to be more mobile than poly(*R*)-(3-hydroxybutyrate) {PHB} in the crystalline regions. The molecular-level evidence by solid state nuclear magnetic resonance (NMR) that the P(HB-HHx) chain is more flexible than PHB is echoed by the dynamic frequency sweep measurements of the biopolymer melts, which show that the PHB melt has an unusual rheological response with the dynamic loss moduli dominating the storage moduli at all frequencies. This is most likely to be caused by the local anisotropic melt structures due to the long persistence length of PHB in the melt. Upon cooling the PHB melt to the solid state, such high levels of anisotropy may be frozen into the solid causing lower chain mobility, and hence giving rise to lower toughness. The incorporation of longer side chain unit to the main chain gives rise to a dynamic rheological response in P(HB-HHx) similar to that of an isotropic melt. This is believed to be due to the enhanced chain flexibility, and hence reduced persistence length. This further allows P(HB-HHx) to be processed into a more uniform isotropic morphology, and hence with improved mechanical toughness.

Keywords: Poly(hydroxyalkanoates); Solid state NMR; Rheology

1. Introduction

Poly(*R*)-(3-hydroxybutyrate-*co*-3-hydroxyhexanoate) {[$-COCH_2CH(CH_3)O-$]$_x$–[$-COCH_2CH(CH_2CH_2CH_3)$-$O-$]$_y$; P(HB-HHx)} is a relatively new biodegradable polymer within the class of natural polyesters called poly(hydroxyalkanoates) [1,2]. It is not being produced in large industrial-scale quantities, and is not commercially available yet. However, P(HB-HHx) has potentially high commercial and practical values because of its improved properties over poly(*R*)-(3-hydroxybutyrate) {[$-COCH_2$-$CH(CH_3)O-$]$_x$; PHB}. P(HB-HHx) has a wider thermal processing window and a longer elongation-at-break than PHB [3–5]. The glass transition temperature (T_g) and the percentage of elongation depend on the mol% of HHx units present in the statistically random copolymer chain or, more generally, depend on the average number of carbon atoms in the side-chain [5,6]. Copolymers that have on average more than 4 carbon atoms in the side-chain, such as those with octanoate, nonanoate or decanoate units are elastomers at room temperature, and they behave as tacky gels during solvent extraction from bacteria cells.

Poly(*R*)-(3-hydroxybutyrate-*co*-3-hydroxyvalerate) {[$-COCH_2CH(CH_3)O-$]$_x$–[$-COCH_2CH(CH_2CH_3)O-$]$_y$; P(HB-HV)} and P(HB-HHx) have all the characteristics of conventional semi-crystalline thermoplastics, such as melting and crystallization temperatures, yield point and plastic deformation in the stress-strain curve, and X-ray diffraction patterns [3–11]. Efforts had also been attempted to produce poly(hydroxyalkanoates) from renewable agricultural products and processed-food industrial wastes [12–16].

Cocrystallization of P(HB-HV), and phase segregation of PHB/P(HB-HV) blends has been studied recently with both

---

[*] Corresponding author. Fax: +852-2364-9932.
E-mail address: bckcheung@polyu.edu.hk (M.K. Cheung).

0032-3861/03/$ - see front matter © 2003 Elsevier Science Ltd. All rights reserved.
doi:10.1016/S0032-3861(03)00222-2

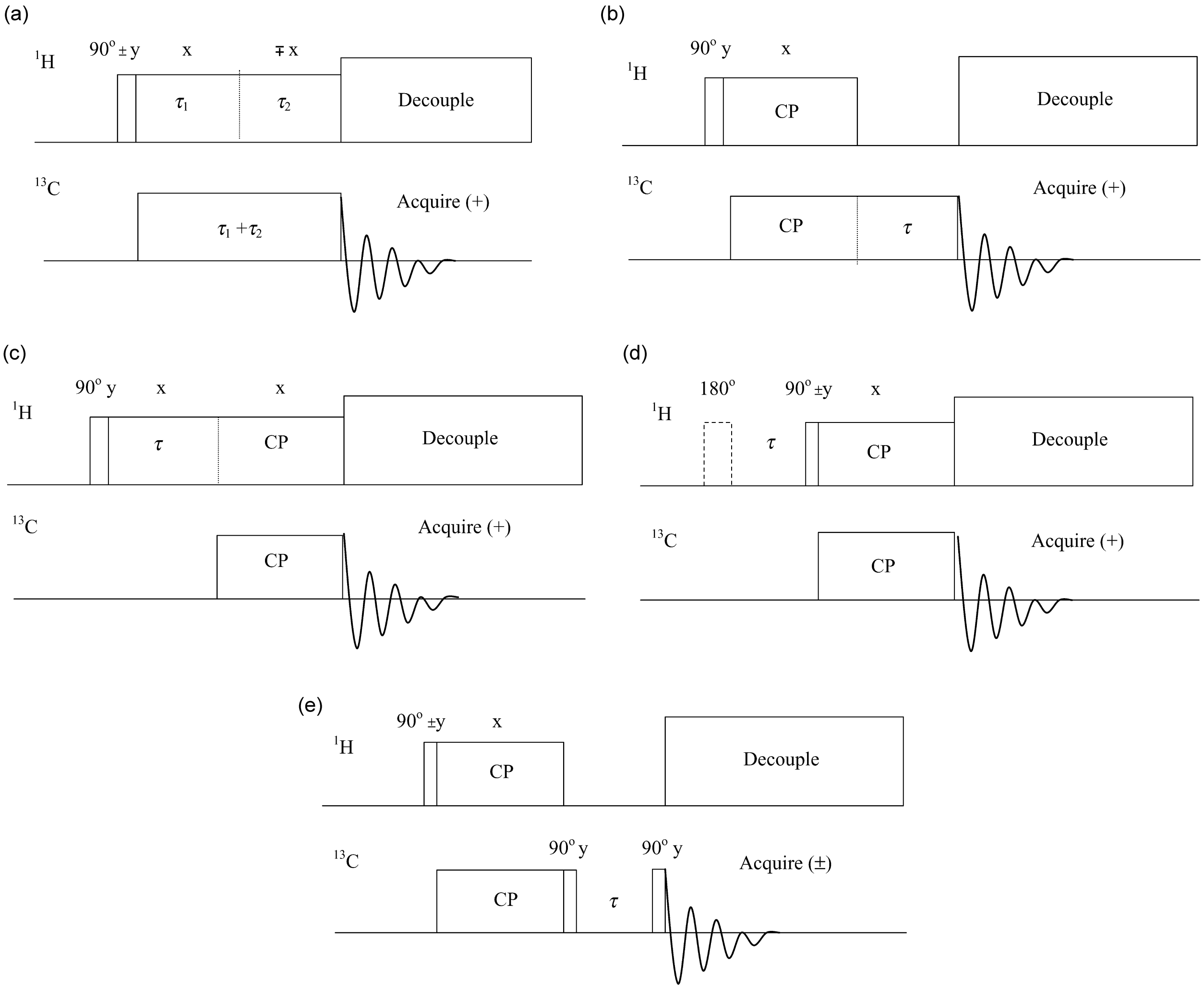

Fig. 1. (a) SLCP sequence. The proton phase during τ_2 is 180° phase shifted from that during τ_1 for odd numbered scans but remains at the same phase as that during τ_1 for even numbered scans. The phases of the proton 90°-pulse for pairs of consecutive odd/even numbered scans are 180° phase shifted accordingly. (b) Carbon spin-lock $^{\mathrm{C}}T_{1\rho}$ sequence. (c) Proton spin-lock $^{\mathrm{H}}T_{1\rho}$ sequence. (d) Freeman–Hill proton spin-lattice relaxation $^{\mathrm{H}}T_1$ sequence. The 180°-pulse is only pulsed during odd numbered scans. (e) Torchia carbon spin-lattice relaxation $^{\mathrm{C}}T_1$ sequence. The proton 90°-pulse, in conjunction with the receiver, is 180° phase shifted accordingly for pairs of consecutive odd/even numbered scans. (+) and (−) during acquisition refer to alternate adding and subtracting data into memory.

differential scanning calorimetry (DSC) and cross-polarization with magic-angle sample spinning (CP/MAS) [17–19]. The protonated carbons peaks in CP/MAS spectra were deconvoluted into crystalline and amorphous resonances. The degrees of crystallinity were estimated to be about 60–70% [18,19]. The mol% of the minor HV comonomer unit within the major HB crystallite was lower than the overall mol% of HV in the whole copolymer [17–21]. PHB and P(HB-HV) copolymer that contained fewer than 10 mol% of HV could form cocrystals in the blends [19]. Whereas, multiple melting temperature (T_{m}) peaks, which indicate phase segregation, were observed in the DSC melting thermograms of blends of PHB and P(HB-HV) with above 20 mol% HV.

This paper concerns mainly nuclear magnetic resonance (NMR) relaxation measurements of solid PHB and P(HB-HHx) at ambient temperature. Previous molecular dynamics studies were dominated by ^{13}C spin-lattice relaxation ($^{\mathrm{C}}T_1$) and line width measurements [22]. $^{\mathrm{C}}T_1$ is sensitive to local segmental motions in the 10–100 MHz range, but it is the cooperative backbone motions in the 1–100 kHz range that determine the macroscopic mechanical properties of polymers. An alternative cross-polarization/depolarization (CP/DP) sequence is proposed here. The original CP/DP sequence was for spectral editing and for determining the degree of crystallinity on the basis of the differences in cross-relaxation time (T_{CH}) [23–26]. The original sequence was also known as inversion-recovery cross-polarization (IRCP) because the observed signals underwent inversion-recovery [24]. The sequence proposed here yields instead signals that decay to zero. T_{CH} was known to correlate with mechanical properties, such as dynamic storage modulus, loss modulus, and impact strength [27–31]. The present study provides microscopic evidence that P(HB-HHx) is

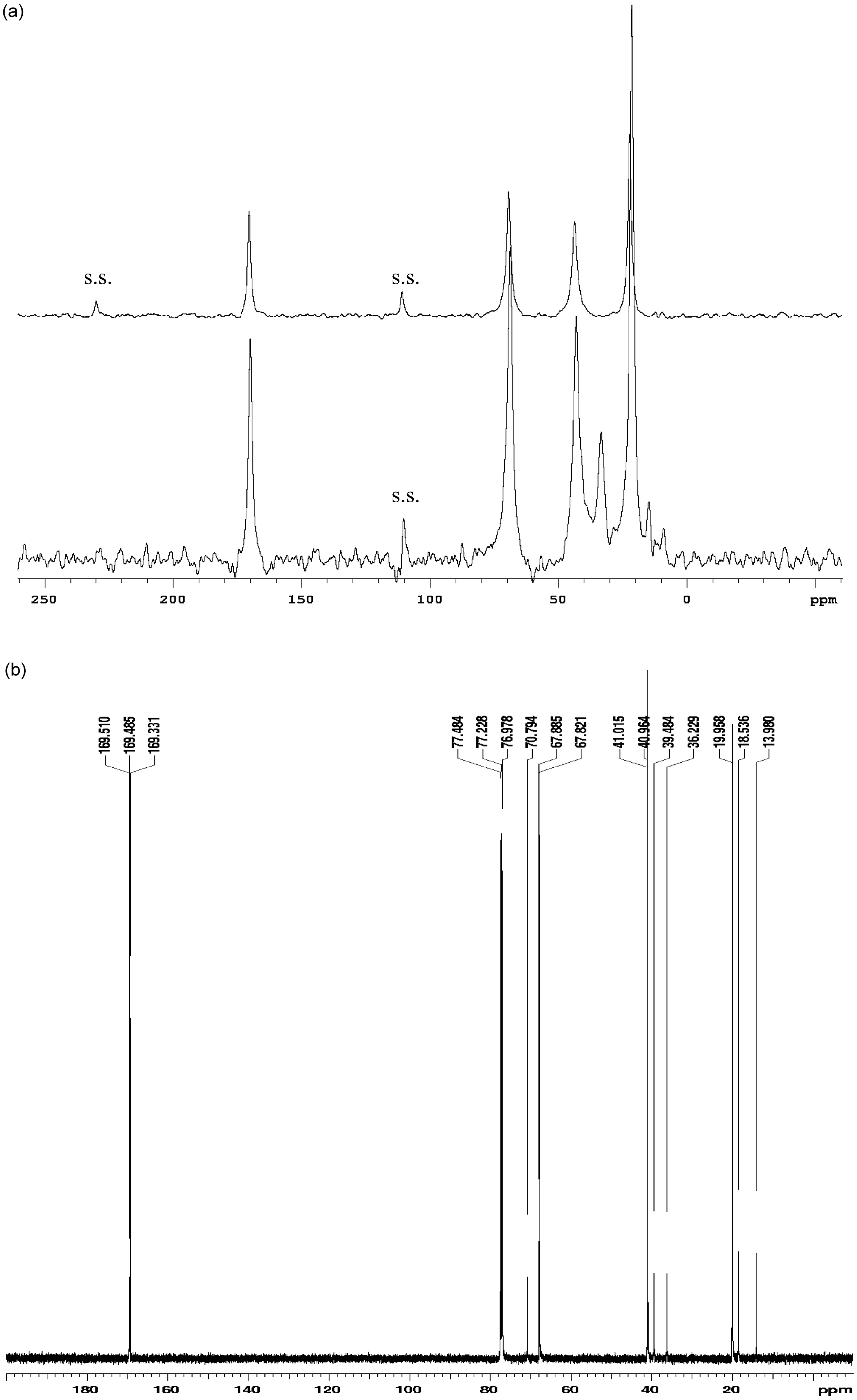

Fig. 2. (a) ^{13}C CP/MAS spectra of PHB (top) and P(HB-HHx) (bottom) at MAS rate of 6 kHz. s.s. stands for spinning sidebands. (b) ^{13}C NMR with proton decoupling spectrum of P(HB-HHx) dissolved in $CDCl_3$ acquired with a Varian INOVA™ 500 MHz spectrometer.

tougher than PHB because the copolymer chain is more flexible, and so is able to dissipate high-speed impact energy better, and to shear yield during slow tensile deformation.

2. Experimental section

Biosynthesized PHB was purchased from Fluka (product # 81329). The weight-average molecular weight (*M*w) of PHB according to the supplier was 400–700 kDa. P(HB-HHx) was biosynthesized at Tsinghua University in Beijing, China with bacterial strain *Pseudomonas stutzeri* 1317 in a glucose mineral-salt medium [2]. The molar ratio of HB/HHx (85:15) was determined with a gas chromatography procedure, which involves dissolving the P(HB-HHx) in an esterification liquid mixture [2]. The M_w of P(HB-HHx) was about 750 kDa. The melting temperature (T_m) of PHB and P(HB-HHx) measured with DSC during the first heating scan at 10 °C/min were 179 and 109 °C, respectively [3]. The glass transition temperature (T_g) of PHB and P(HB-HHx) measured during the second DSC heating scan at 10 °C/min were 5.7 and 3.2 °C, respectively [3].

Cross-polarization with magic-angle sample spinning (CP/MAS) measurements were made at ambient temperature (23 °C) using a Varian INOVA™ high-power, wide-bore, 400 MHz spectrometer. The samples were placed into 7.5 mm Chemagnetics™ Pencil™ rotors. The spinning rates were stable within ± 1 Hz. The pre-delay recycle time was 5.0 s. The ^{1}H 90° pulse width was 5.0 μs, and the spin-lock (SL) field was 50 kHz. The ^{13}C SL field was 45 kHz. The CP contact-time was 1.0 ms. The ^{13}C chemical shift scale was set using a solid external reference, hexamethylbenzene (HMB). The CH_3 groups of HMB resonate at 17.35 ppm relative to tetramethylsilane (TMS).

The CP time constant (T_{CH}) was measured with the sequence in Fig. 1(a), which is a modified form of the IRCP sequence. The modified scheme yields signals that decay to zero, and so may be known instead as the spin lock decay cross-polarization (SLCP) sequence. The measurements were done with 20 τ_2 values from 3 to 3000 μs.

Carbon rotating-frame relaxation time ($^{C}T^*_{1\rho}$) and proton rotating-frame relaxation time ($^{H}T_{1\rho}$) were measured with the sequences in Fig. 1(b) and (c), respectively. The $^{C}T^*_{1\rho}$ and $^{H}T_{1\rho}$ measurements were done with 20 τ values from 0.1 to 30 ms.

Proton spin-lattice relaxation time ($^{H}T_1$) and carbon spin-lattice relaxation time ($^{C}T_1$) were measured with the Freeman–Hill and Torchia sequences in Fig. 1(d) and (e), respectively. The sequences were modified in such a way so that the measured signals decay to zero instead of displaying inversion-recovery. The advantages that associate with the decay to zero approach have been reviewed [32]. All four sequences used in this work employ quadrature phase cycling to suppress electronic noise and artifacts.

The dynamic frequency sweeps measurements were performed in the linear viscoelastic region with Rheometrics Mechanical Spectrometer, RMS 800. The 25 mm diameter parallel plate fixture was used for all testing. The samples were first dried in vacuum at 80 °C for 24 h to remove moisture or any solvent residue. The dried samples were then compressed into 0.5 mm thick 25 mm diameter discs. The compression temperature for the pure PHB was 185 °C while for P(HB-HHx) was 150 °C. The experimental protocol was as follows: the system was equilibrated at 185 °C for at least 20 min. The PHB sample was then loaded in between the parallel plate fixture and maintained at this temperature for about 5 min. The sample was subsequently cooled to 150 °C and re-equilibrated at this temperature for another 5 min. The strain sweeps and frequency sweeps were carried out at 150 °C. The P(HB-HHx) melt was simply equilibrated at 150 °C for measurements. The above protocol was developed based on the strong supercooling response of PHB. DSC showed that PHB crystallizes at about 100 °C on cooling from the molten state. The use of such protocol ensures that thermal degradation is minimized.

3. Results and discussion

Fig. 2(a) shows the CP/MAS spectra of PHB (top) and P(HB-HHx) (bottom). Both spectra clearly show the four carbons in the HB monomer unit, which may be assigned by referring to the ^{13}C liquid NMR spectrum of P(HB-HHx) in Fig. 2(b). The HB resonant peaks relative to TMS are CH_3 (21 ppm), CH_2 (43 ppm), CH (69 ppm), and C=O (170 ppm). The C=O resonance of HHx overlap with that of HB at 170 ppm. The

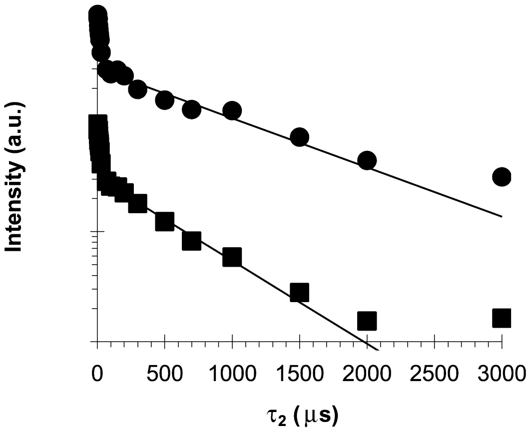

Fig. 3. Solid circles denote (M/M_0) vs τ_2 data measured with SLCP, and solid squares denote ($M_0 - M$)/2M_0 vs τ_2 data measured with IRCP at the CH_2 resonance (43 ppm) of PHB at MAS rate of 6 kHz. Both methods give similar short T_{CH} components, 18 μs (72%) for SLCP and 17 μs (71%) for IRCP, but give different long T_{CH} values, 970 μs (28%) for SLCP and 580 μs (29%) for IRCP. The discrepancy arises probably because $|M(\tau_2 = 0)| > |M(\tau_2 \rightarrow \infty)| \neq M_0$ causing a serious systematic error with the IRCP method.

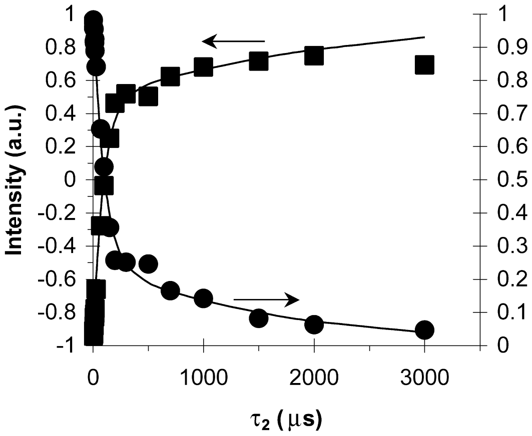

Fig. 4. Solid squares show that the IRCP of CH_3 group (21 ppm) of P(HB-HHx) at MAS rate of 6 kHz suffers from ${}^{H}T_{1\rho}$ effect at long τ_2. Solid circles show that SLCP does not suffer from ${}^{H}T_{1\rho}$ effect as much because T_{CH} decay dominates according to Eq. (4) Note also that $|M(\tau_2 = 0)| > |M(\tau_2 \rightarrow \infty)| \neq M_0$ in IRCP.

relaxation times are measured at 21, 43, and 69 ppm. The CH_2 (33 ppm) group in the main-chain of the HHx unit is clearly resolved but the flexible side-chain groups in the 10–20 ppm range are barely distinguishable from the baseline noise.

The cross-relaxation time (T_{CH}) can be measured with a conventional SL Hartmann–Hahn CP sequence by varying the contact time. The recovery of the carbon magnetization in most solid polymers usually follows the equation [33,34]:

$$M = M_0 \exp\left(-\frac{\tau}{{}^{H}T_{1\rho}}\right)\left\{1 - \exp\left(-\frac{\tau}{T_{CH}}\right)\right\} \tag{1}$$

The effect of ${}^{H}T_{1\rho}$ may be ignored at very short contact times because $\tau \ll {}^{H}T_{1\rho}$, and so the magnetization is recovered similar to T_1 saturation-recovery. On the other hand, ${}^{H}T_{1\rho}$ is usually measured at long contact times. T_{CH} may also be measured by inversion-recovery with an IRCP sequence (the proton phase during τ_2 is 180° phase shifted from that during τ_1). The contact time τ_1 for most solid polymers is usually about 1–3 ms. Therefore, the carbon magnetization recovers according to [23–25]

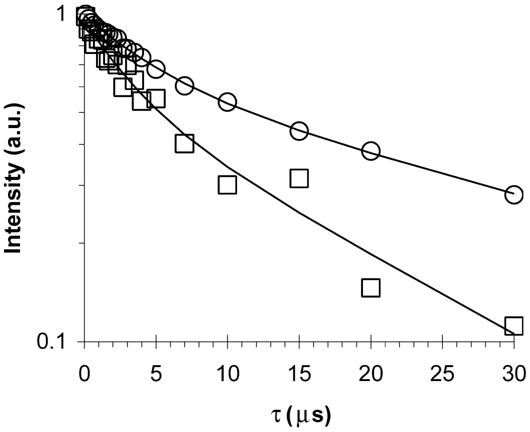

Fig. 5. ${}^{C}T^{*}_{1\rho}$ relaxation of CH_2 group (43 ppm) of PHB (open circles) and P(HB-HHx) (open squares) at MAS rate of 4 kHz.

$$M = \left\{M_0 \exp\left(-\frac{\tau_1 + \tau_2}{{}^{H}T_{1\rho}}\right)\right\} \times \left\{1 + \exp\left(-\frac{\tau_1 + \tau_2}{T_{CH}}\right) - 2\exp\left(-\frac{\tau_2}{T_{CH}}\right)\right\} \tag{2}$$

The carbon magnetization recovery for a two-component T_{CH} system may be rearranged for the limiting case of $\tau_1 \gg T_{CH}$ and $(\tau_1 + \tau_2) < {}^{H}T_{1\rho}$, which is met in most thermoplastics, such as in our PHB and P(HB-HHx), at room temperature [24]:

$$\frac{M_0 - M}{2M_0} \approx \phi_A \exp\left(-\frac{\tau_2}{T^{A}_{CH}}\right) + (1 - \phi_A)\exp\left(-\frac{\tau_2}{T^{B}_{CH}}\right) \tag{3}$$

The proposed pulse sequence in Fig. 1(a) may be abbreviated as SLCP because it effectively subtracts Eq. (2) from Eq. (1) to yield an exponential or SL decay of the carbon magnetization for the case of $\tau_1 \gg T_{CH}$ and $(\tau_1 + \tau_2) < {}^{H}T_{1\rho}$:

$$\frac{M}{M_0} \approx \phi_A \exp\left(-\frac{\tau_2}{T^{A}_{CH}}\right) + (1 - \phi_A)\exp\left(-\frac{\tau_2}{T^{B}_{CH}}\right) \tag{4}$$

Table 1
Cross-relaxation time (T_{CH}) measured at spinning rates of 4 and 6 kHz. The T_{CH} relaxation curves are fitted to two exponential decay components. The fractions of the two components are indicated in parentheses as percentages

Functional group		PHB		P(HB-HHx)	
		4 kHz	6 kHz	4 kHz	6 kHz
CH_2	Fast	14 μs (66%)	18 μs (72%)	22 μs (72%)	23 μs (71%)
	Slow	520 μs (34%)	970 μs (28%)	810 μs (28%)	970 μs (29%)
	$1/\langle T_{CH}^{-1}\rangle$	21 μs	25 μs	30 μs	32 μs
CH	Fast	21 μs (57%)	23 μs (60%)	30 μs (62%)	27 μs (60%)
	Slow	530 μs (43%)	1030 μs (40%)	680 μs (38%)	1250 μs (40%)
	$1/\langle T_{CH}^{-1}\rangle$	35 μs	38 μs	47 μs	44 μs
CH_3	Fast	84 μs (66%)	80 μs (66%)	77 μs (63%)	97 μs (75%)
	Slow	1010 μs (34%)	1610 μs (34%)	1080 μs (37%)	1620 μs (25%)
	$1/\langle T_{CH}^{-1}\rangle$	120 μs	120 μs	120 μs	130 μs

Table 2
The apparent ^{13}C spin-lattice relaxation time in the rotating-frame ($^{C}T_{1\rho}^{*}$) measured at spinning rates of 4 and 6 kHz. The $^{C}T_{1\rho}^{*}$ relaxation curves are fitted to two exponential decay components. The fractions of the two components are indicated in parentheses as percentages

Functional group		PHB		P(HB-HHx)	
		4 kHz	6 kHz	4 kHz	6 kHz
CH_2	Fast	5.1 ms (36%)	2.8 ms (38%)	3.4 ms (42%)	1.8 ms (76%)
	Slow	37 ms (64%)	13 ms (62%)	18 ms (58%)	11 ms (24%)
	$1/\langle {}^{C}T_{1\rho}^{*-1}\rangle$	11 ms	5.5 ms	6.4 ms	2.3 ms
CH	Fast	3.8 ms (14%)	4.5 ms (25%)	1.6 ms (18%)	1.0 ms (47%)
	Slow	78 ms (86%)	43 ms (75%)	38 ms (82%)	23 ms (53%)
	$1/\langle {}^{C}T_{1\rho}^{*-1}\rangle$	21 ms	14 ms	7.4 ms	2.0 ms
CH_3	Fast	9.5 ms (17%)	8.1 ms (21%)	6.5 ms (33%)	2.4 ms (39%)
	Slow	140 ms (83%)	74 ms (79%)	110 ms (67%)	41 ms (61%)
	$1/\langle {}^{C}T_{1\rho}^{*-1}\rangle$	41 ms	27 ms	18 ms	5.7 ms

Fig. 3 shows the typical way to calculate the two T_{CH} components from IRCP and SLCP using Eqs. (3) and (4), respectively. SLCP is more advantageous because, in practice, the least squares fit to the semi-log plot of M/M_0 vs τ_2 yields the two T_{CH} components directly. However, in Eq. (3) the linearized form of IRCP assumes that $|M(\tau_2 = 0)| = |M(\tau_2 \to \infty)| = M_0$, but this is not true because of CP enhancement of $|M(\tau_2 = 0)|$ and $^{H}T_{1\rho}$ reduction of $|M(\tau_2 \to \infty)|$. Fig. 4 presents the IRCP and SLCP data of P(HB-HHx) at MAS rate of 6 kHz to demonstrate that SLCP is not as susceptible as IRCP to the effect of $^{H}T_{1\rho}$ at long τ_2. The T_{CH} components and their percentages, which are measured with SLCP, are listed in Table 1. The average cross-relaxation rate $\langle T_{CH}^{-1}\rangle$ and the other average relaxation rates, namely $\langle {}^{C}T_{1\rho}^{*-1}\rangle$ and $\langle {}^{C}T_{1}^{-1}\rangle$, are calculated by simple weight averaging:

$$\langle T_x^{-1}\rangle = \frac{\phi_A}{T_x^A} + \frac{(1-\phi_A)}{T_x^B} \tag{5}$$

The fast T_{CH} component detected in the biopolymers belong to protons that are directly bonded to those ^{13}C within rigid ordered domains.

The experimentally detected carbon spin-lattice relaxation times in the rotating-frame ($^{C}T_{1\rho}^{*}$) are listed in Table 2. Fig. 5 shows that P(HB-HHx) $^{C}T_{1\rho}^{*}$ decays faster than PHB, which indicates that the copolymer is more flexible. Proton rotating-frame relaxation times ($^{H}T_{1\rho}$) listed in Table 3 confirms that P(HB-HHx) is more flexible.

Table 3
^{1}H spin-lattice relaxation time in the rotating-frame ($^{H}T_{1\rho}$) measured at spinning rates of 4 and 6 kHz. The $^{H}T_{1\rho}$ relaxation curves are adequately regarded as single exponential because proton spin diffusion tends to average out any $^{H}T_{1\rho}$ dispersion

Functional group	PHB		P(HB-HHx)	
	4 kHz	6 kHz	4 kHz	6 kHz
CH_2	42 ms	38 ms	12 ms	9.7 ms
CH	41 ms	37 ms	11 ms	10 ms
CH_3	40 ms	35 ms	12 ms	8.9 ms

The $^{C}T_{1\rho}^{*}$ decay curves of the biopolymers are generally well characterized as bi-exponential. $^{C}T_{1\rho}^{*}$ is the carbon rotating-frame relaxation time measured at 45 kHz ^{13}C SL field at ambient temperature. The measured $^{C}T_{1\rho}^{*}$ contains significant enough motional information so that the more mobile P(HB-HHx) chain is clearly distinguished from PHB with a faster $\langle {}^{C}T_{1\rho}^{*-1}\rangle$. Table 2 shows that the percentages of slow and fast $^{C}T_{1\rho}^{*}$ components differed at different carbon groups because $^{C}T_{1\rho}^{*}$ depends on both the local bonding environments and the local flexibilities [31,35–37].

The long-range cooperative backbone mobility is best measured at CH_2 (43 ppm) or CH (69 ppm). Both $^{C}T_{1\rho}^{*-1}$ and $^{H}T_{1\rho}^{*-1}$ relaxation rates contain motional information in the 10–100 kHz range, which determines the macroscopic mechanical properties of polymers. $\langle {}^{C}T_{1\rho}^{*-1}\rangle$ and $^{H}T_{1\rho}^{*-1}$ become faster with increasing MAS rate, which may be due to the introduction of additional modes of motion in the kHz range as extra sources of relaxation.

Proton spin diffusion averages both $^{H}T_{1\rho}$ and $^{H}T_{1}$, as seen in the single exponential decays of Figs. 6 and 7. The slow spin diffusion of ^{13}C in its natural abundance allows $^{C}T_{1}$ to contain local motional information near the Larmor frequency. Sidebands on either side of the C=O peak

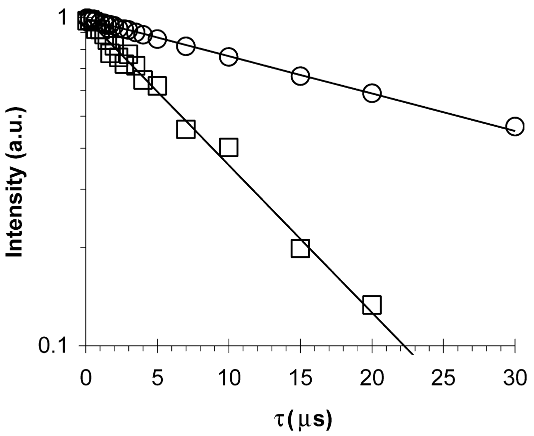

Fig. 6. $^{H}T_{1\rho}$ relaxation of CH_2 group (43 ppm) of PHB (open circles) and P(HB-HHx) (open squares) at MAS rate of 6 kHz.

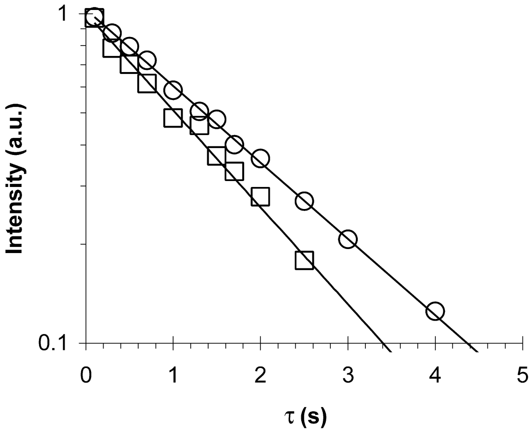

Fig. 7. $^{H}T_1$ relaxation of CH_2 group (43 ppm) of PHB (open circles) and P(HB-HHx) (open squares) at MAS rate of 6 kHz.

(170 ppm) can still be seen at MAS rate of 6 kHz. CH_3 is quite mobile, and its $^{C}T_1$ is averaged to a magnitude close to its $^{H}T_1$. The source of $^{H}T_1$ and $^{C}T_1$ relaxation is probably the rapidly rotating CH_3 group. Fig. 8 shows typical $^{C}T_1$ relaxation curves of the biopolymers. $1/\langle {}^{C}T_1^{-1}\rangle$ of CH in PHB is shorter than that of the CH_2 because CH is the nearest neighbor of CH_3. However, $1/\langle {}^{C}T_1^{-1}\rangle$ of the CH and CH_2 groups in PHB differ only within 20% at MAS rate of 6 kHz. Whereas, $1/\langle {}^{C}T_1^{-1}\rangle$ of the CH and CH_2 groups in the more mobile P(HB-HHx) are averaged to within 20% at both MAS rates of 4 and 6 kHz. Tables 4 and 5 list the $^{H}T_1$ and $^{C}T_1$ measurements, respectively.

For semi-crystalline polymers to be considered as tough, they must be able to display yielding and plastic deformation [38]. The polymer chain must be flexible on the molecular level so that the material is tough on the macroscopic level [39,40]. Adding a co-monomer like HHx into the backbone of PHB is one possible way to increase the toughness of this kind of biopolymer [5,6]. The longer flexible side-chain of the HHx unit, which is distributed randomly throughout the backbone, probably increases the free volume in the amorphous regions, weakens the crystallites, and results in smaller crystallites. A previous study of P(HB-HHx) reported that T_g decreases and elongation-at-break increases with increasing number of HHx units [5]. The ratio of T_{CH} to ${}^{C}T_{1\rho}^{*}$ for backbone carbons was found to correlate directly with the impact strength of glassy polymers at ambient temperature [31]. Likewise, Table 6 shows that the ratios of $1/\langle T_{CH}^{*-1}\rangle$ (in μs) to $1/\langle {}^{C}T_{1\rho}^{*-1}\rangle$ (in ms) for the backbone CH_2 group of P(HB-HHx) and PHB, at MAS rate of 4 kHz, are 4.7 and 1.9, respectively. Whereas, the ratios at MAS rate of 6 kHz are 14 and 4.5 for the backbone CH_2 group of P(HB-HHx) and PHB, respectively.

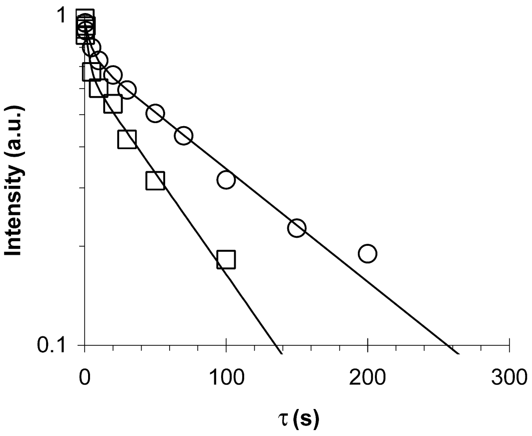

Fig. 8. $^{C}T_1$ relaxation of CH_2 group (43 ppm) of PHB (open circles) and P(HB-HHx) (open squares) at MAS rate of 6 kHz.

Table 4
^{1}H spin-lattice relaxation time ($^{H}T_1$) measured at spinning rates of 4 and 6 kHz. The $^{H}T_1$ relaxation curves are single exponential because of proton spin diffusion

Functional group	PHB		P(HB-HHx)	
	4 kHz	6 kHz	4 kHz	6 kHz
CH_2	1.9 s	2.2 s	1.3 s	1.5 s
CH	1.9 s	2.2 s	1.3 s	1.5 s
CH_3	1.8 s	2.0 s	1.5 s	1.2 s

Linear viscoelastic responses of the molten PHB and P(HB-HHx) are depicted in Figs. 9 and 10, respectively. The dynamic modulus of PHB is predominantly dominated by the viscous responses over the entire frequency spectrum. P(HB-HHx) displays a similar response to an isotropic melt with the loss modulus dominating the storage modulus at all frequencies tested. However, there is a tendency for the storage modulus of P(HB-HHx) to become dominant at higher frequencies. In addition, the loss modulus of P(HB-HHx) shows a perfect terminal response, i.e. it is proportional to frequency. On the other hand, the storage modulus of P(HB-HHx) nearly exhibits a terminal response, it is proportional to the square of the frequency.

The unusual liquid crystalline-like response from PHB was also reported before [41]. However, all reported data were obtained at temperatures where PHB thermal

Table 5
^{13}C spin-lattice relaxation time ($^{C}T_1$) measured at spinning rates of 4 and 6 kHz. The $^{C}T_1$ relaxation curves are bi-exponential decay except for that of the CH_3 group, which is single exponential

Functional group		PHB		P(HB-HHx)	
		4 kHz	6 kHz	4 kHz	6 kHz
CH_2	Fast	15 s (28%)	5.1 s (21%)	13 s (56%)	3.5 s (32%)
	Slow	170 s (72%)	130 s (79%)	180 s (44%)	83 s (68%)
	$1/\langle {}^{C}T_1^{-1}\rangle$	44 s	21 s	21 s	10 s
CH	Fast	8.2 s (31%)	5.3 s (25%)	6.5 s (19%)	4.8 s (33%)
	Slow	95 s (69%)	96 s (75%)	42 s (81%)	61 s (67%)
	$1/\langle {}^{C}T_1^{-1}\rangle$	22 s	18 s	20 s	12 s
CH_3		2.4 s	2.5 s	1.6 s	1.6 s

Table 6
The ratio of $\langle {}^{\mathrm{C}}T_{1_\rho}^{*-1} \rangle$ to $\langle T_{\mathrm{CH}}^{-1} \rangle$ as an indicator of the chain mobility and mechanical toughness in thermoplastics as proposed in reference 31. It follows that P(HB-HHx) is probably more flexible and mechanically tougher than PHB

Functional group	PHB		P(HB-HHx)	
	4 kHz	6 kHz	4 kHz	6 kHz
CH_2 $\langle {}^{\mathrm{C}}T_{1_\rho}^{*-1} \rangle / \langle T_{\mathrm{CH}}^{-1} \rangle \times 10^3$	1.9	4.5	4.7	14
CH $\langle {}^{\mathrm{C}}T_{1_\rho}^{*-1} \rangle / \langle T_{\mathrm{CH}}^{-1} \rangle \times 10^3$	1.7	2.7	6.4	22
CH_3 $\langle {}^{\mathrm{C}}T_{1_\rho}^{*-1} \rangle / \langle T_{\mathrm{CH}}^{-1} \rangle \times 10^3$	2.9	4.4	6.7	23

degradation was unavoidable, and so it was not easy to attribute the responses to either molecular intrinsic features or reduction in molecular weight of the material by thermal degradation. By making use of the strong supercooling response of the material, we were able to perform the rheological measurements far below the thermal degradation temperature, and hence probe the molecular structure effects with melt rheology. We believe that the strong viscous response is due to the local orientational order of PHB. Neutron scattering measurements have shown that PHB has a very high degree of local chain persistence, although the material's global response is still Gaussian [42]. The local anisotropy detected in the melt is then likely to be frozen into the final cooled solid product, and hence gives rise to an enhanced Young's modulus, but with reduced toughness. The ease of retaining local molecular ordering could also be responsible for the strong permeability resistance exhibited by the material [43].

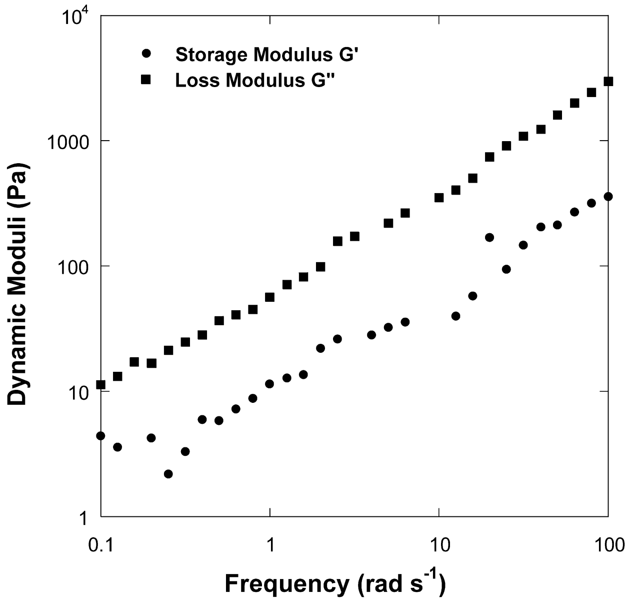

Fig. 9. Dynamic frequency sweep on PHB samples using a parallel plate fixture of 25 mm diameter and a gap of 0.5 mm at 150 °C. The sample was melted and kept isothermally for 20 min at 185 °C prior to cooling to 150 °C.

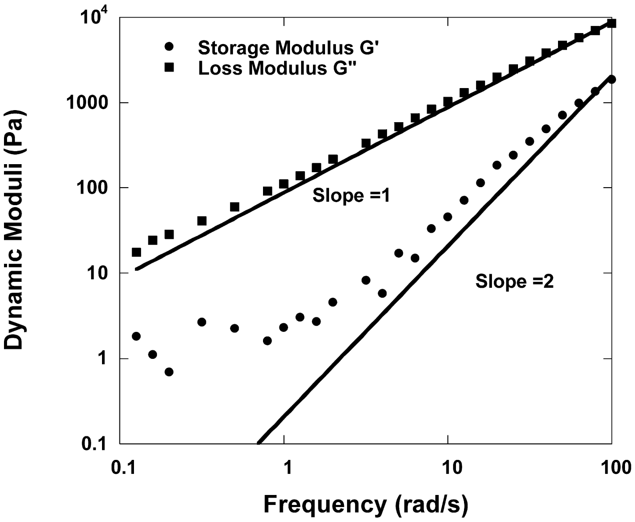

Fig. 10. Dynamic frequency sweep on copolymer P(HB-HHx) samples using a parallel plate fixture of 25 mm diameter and a gap of 0.5 mm at 150 °C.

4. Conclusions

The proposed SLCP sequence is suitable for measuring T_{CH} in semi-crystalline polymers. The ratio of $\langle {}^{\mathrm{C}}T_{1\rho}^{*-1} \rangle / \langle T_{\mathrm{CH}}^{-1} \rangle$ is at least 2–3 times larger in P(HB-HHx) than in PHB, which indicates that P(HB-HHx) is relatively more flexible in the crystalline regions.

By incorporating the bulky side chain group into the main chain, the long-range chiral packing becomes difficult, and hence a classical melt rheology is exhibited instead in the copolymer melt. PHB melt, on the other hand, shows liquid crystalline-like viscoelastic responses indicative of local anisotropic melt structures, which may be frozen into the solid state upon cooling giving rise to stiff, but brittle final products.

Acknowledgements

Financial supports from the Hong Kong Research Grant Council for grant # PolyU 5299/01P, grant # HKUST6230/01P, and from the University Grants Committee Area of Excellence Scheme (Hong Kong) AoE/P-10/01 are greatly appreciated. The P(HB-HHx) sample generously provided by Prof. George Guo-qiang Chen of Tsinghua University, Beijing, made this study possible.

References

[1] Kato M, Bao HJ, Kang CK, Fukui T, Doi Y. Appl Microbiol Biotechnol 1996;45:363–70.

[2] Xi J, Wu Q, Yan Y, Zhang Z, Yu PHF, Cheung MK, Zhang R, Chen GQ. Antonie van Leeuwenhoek 2000;78:43–9.
[3] He JD, Cheung MK, Yu PH, Chen GQ. J Appl Polym Sci 2001;82: 90–8.
[4] Watanabe T, He Y, Fukuchi T, Inoue Y. Macromol Biosci 2001;1: 75–83.
[5] Doi Y, Kitamura S, Abe H. Macromolecules 1995;28:4822–8.
[6] Marchessault RH, Monasterios CJ, Morin FG, Sundararajan PR. Int J Bio Macromol 1990;12:158–65.
[7] Kunioka M, Tamaki A, Doi Y. Macromolecules 1989;22:694–7.
[8] Kunioka M, Doi Y. Macromolecules 1990;23:1933–6.
[9] Pearce R, Marchessault RH. Polymer 1994;35:3990–7.
[10] He Y, Shuai X, Cao A, Kasuya K, Doi Y, Inoue Y. Polym Degrad Stab 2001;73:193–9.
[11] Yamada S, Wang Y, Asakawa N, Yoshie N, Inoue Y. Macromolecules 2001;34:4659–61.
[12] Wong HH, Lee SY. Appl Microbiol Biotechnol 1998;50:30–3.
[13] Liu F, Li WQ, Ridgway D, Gu TY, Shen ZY. Biotechnol Lett 1998; 20:345–8.
[14] Ramsay JA, Hassan MCA, Ramsay BA. Can J Microbiol 1995;41: 262–6.
[15] Kim BS, Chang HN. Biotechnol Lett 1998;20:109–12.
[16] Yu PH, Chua H, Huang AL, Lo W, Chen GQ. Appl Biochem Biotechnol 1998;70:603–14.
[17] VanderHart DL, Orts WJ, Marchessault RH. Macromolecules 1995; 28:6394–400.
[18] Kamiya N, Sakurai M, Inoue Y, Chûjô R, Doi Y. Macromolecules 1991;24:2178–82.
[19] Saito M, Inoue Y, Yoshie N. Polymer 2001;42:5573–80.
[20] Yoshie N, Fujiwara M, Ohmori M, Inoue Y. Polymer 2001;42: 8557–63.
[21] Yoshie N, Sakurai M, Inoue Y, Chûjô R. Macromolecules 1992;25: 2046–8.
[22] Inoue Y. In: Ando I, Asakura T, editors. Solid state NMR of polymers. Amsterdam: Elsevier; 1998. p. 771–817.
[23] Melchior MT. 22nd Experimental NMR conference, Poster B-29, Asilomar, CA, April 1981.
[24] Cory DG, Ritchey WM. Macromolecules 1989;22:1611–5.
[25] Sangill R, Rastrup-Andersen N, Bildsøe H, Jakobsen HJ, Nielsen NC. J Magn Reson A 1994;107:67–78.
[26] Wu X, Burns ST, Zilm KW. J Magn Reson A 1994;111:29–36.
[27] Parker AA, Marcinko JJ, Shieh YT, Hedrick DP, Ritchey WM. J Appl Polym Sci 1990;40:1717–25.
[28] Marcinko JJ, Parker AA, Shieh YT, Ritchey WM. J Appl Polym Sci 1992;45:391–8.
[29] Parker AA, Marcinko JJ, Rinaldi P, Hedrick DP, Ritchey WM. J Appl Polym Sci 1993;48:677–81.
[30] Marcinko JJ, Parker AA, Rinaldi PL, Ritchey WM. J Appl Polym Sci 1994;51:1777–80.
[31] Schaefer J, Stejskal EO, Buchdahl R. Macromolecules 1977;10: 384–405.
[32] Frye JS. Concepts Magn Reson 1989;1:27–33.
[33] Komoroski RA. In: Komoroski RA, editor. High resolution NMR spectroscopy of synthetic polymers in bulk. Deerfield Beach, FL: VCH Publishers; 1986. p. 19–62.
[34] Mehring M. Principles of high resolution NMR in solids, 2nd, Revised, Enlarged ed. Berlin: Springer; 1983. p. 129–185.
[35] VanderHart DL, Garroway AN. J Chem Phys 1979;71:2773–87.
[36] Schaefer J, Stejskal EO, Steger TR, Sefcik MD, McKay RA. Macromolecules 1980;13:1121–6.
[37] Schaefer J, Sefcik MD, Stejskal EO, McKay RA. Macromolecules 1984;17:1118–24.
[38] Painter PC, Coleman MM. Fundamentals of polymer science, 2 ed. Lancaster, PA: Technomic Publishing Company; 1997. p. 408–12.
[39] Steger TR, Schaefer J, Stejskal EO, McKay RA. Macromolecules 1980;13:1127–32.
[40] Sefcik MD, Schaefer J, Stejskal EO, McKay RA. Macromolecules 1980;13:1132–7.
[41] Choi HJ, Park SH, Yoon JS, Lee HS, Choi SJ. Polym Engng Sci 1995; 35:1636–42.
[42] Beaucage G, Rane S, Sukumaran S, Satkowski MM, Schechtman LA, Doi Y. Macromolecules 1997;30:4158–62.
[43] Bluhm TL, Hamer GK, Marchessault RH, Fyfe CA, Vergin RP. Macromolecules 1986;19:2871–6.